A Case Study of Rossby Wave Breaking along the Subtropical Tropopause

GREGORY A. POSTEL AND MATTHEW H. HITCHMAN

Department of Atmospheric and Oceanic Sciences, University of Wisconsin—Madison, Madison, Wisconsin

(Manuscript received 11 July 2000, in final form 29 March 2001)

ABSTRACT

Global analyses from the European Centre for Medium-Range Weather Forecasts (ECMWF) are used to analyze the sequence of events leading to the creation of a large-scale reversal of potential vorticity (PV) gradients across the subtropical tropopause on 10 June 1992 over the North Pacific. The ''reversed'' (i.e., southward directed) PV gradients across the tropopause initially appeared at 1200 UTC on 10 June, the time herein designated as the ''onset'' of this event, at 25°N near the date line.

Maps of PV are shown to highlight the evolution of a mobile Rossby wave packet during its migration across eastern Asia toward the subtropical Pacific during the several days prior to onset. With explicit regard to the validity of linear theory and the Wentzel–Kramers–Brillouin–Jeffreys approximation, wave activity flux diagnostics are employed to assess the propagation characteristics of this disturbance during that time. Following its departure from eastern Asia, much of the wave activity associated with the packet traveled southeastward along a quasi-horizontal path to the subtropical Pacific, above 300 hPa. A Hovmöller diagram of PV at 350 K is used to estimate the eastward phase speed (c_x) of the PV anomalies in the wave packet during its upper-level transit. The spatial distribution of $\overline{u} - c_x$, where $\overline{u}$ symbolizes the basic-state zonal wind, suggests that the generation of reversed PV gradients over the subtropical Pacific in this case was a result of the wave packet's proximity to a critical line.

The evolution of this disturbance, and its associated production of reversed PV gradients across the tropopause, is viewed in light of previous climatological studies of Rossby wave breaking (RWB) to offer insight into the origin and maintenance of the ''surf zone'' that resides near the subtropical tropopause over the North Pacific during summer. Composites of PV-anomaly patterns and wave activity fluxes, over a set of 33 RWB events that occurred during the 10 boreal summers from 1986 to 1995, imply that this feature is intimately related to repeated critical-layer interactions of the kind exhibited by the 10 June case. Moreover, the entrainment of Asian monsoon outflow into the 10 June PV-gradient reversal (as shown by air-parcel trajectories during the week prior to onset), when placed in the context of previous climatological statistics of the participation of Asian monsoon outflow in similar events, suggests that this surf zone delineates a sector of the atmosphere wherein tropical tropospheric air from the Asian monsoon and relatively high PV from the extratropical stratosphere are united during critical-layer interactions over the subtropical Pacific. These results provide a dynamical framework for understanding complex transport phenomena associated with the outflow of biomass burning and pollution from subtropical continental regions.

1. Introduction

A recent study by Postel and Hitchman (1999, hereafter referred to as PH99) showed that the production of southward-directed (''reversed'') potential vorticity (PV) gradients across the subtropical tropopause occurs nearly exclusively during summer, over the midoceans. These PV configurations, schematically depicted in Fig. 1, are signatures of Rossby wave breaking (RWB) along the tropopause. In general, RWB may be regarded as the rapid (of order 1 day) and irreversible deformation of PV contours (McIntyre and Palmer 1984). It appears as a synoptic-scale, quasi-horizontal analog to the breaking of ocean waves on a beach, whereby PV contours on isentropic surfaces are stretched and folded over in a manner that resembles the bending and twisting of streamlines in a high Reynolds number flow near the wake of a cylinder (e.g., McIntyre and Palmer 1984; Duan and Wiggins 1997). Analytical, numerical, and observational studies (e.g., Stewartson 1978; Warn and Warn 1978; Juckes and McIntyre 1987; Polvani and Plumb 1992; Thorncroft et al. 1993) have shown that the interaction between a Rossby wave and the flow immediately surrounding its critical surface[1] results in

Corresponding author address: Dr. Gregory A. Postel, Department of Atmospheric and Oceanic Sciences, University of Wisconsin—Madison, 1225 W. Dayton Street, Madison, WI 53706.
E-mail: greg@aos.wisc.edu

[1] A critical surface (also referred to as a critical line or a critical level) is the locus of points on which the zonal phase speed of a wave matches the mean zonal flow speed. A critical layer is the region surrounding a critical surface, wherein wave transience, dissipation, and/or nonlinearity are important processes in the flow's evolution (e.g., Andrews et al. 1987).

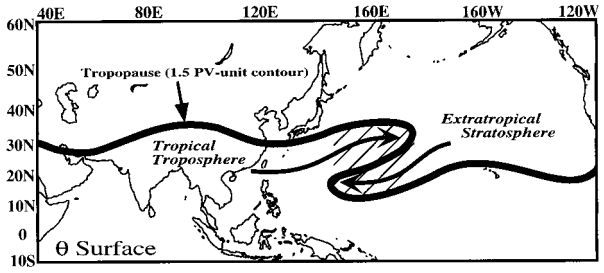

FIG. 1. Schematic of Rossby wave breaking along the tropopause on an upper-level isentropic (θ) surface over the North Pacific Ocean. The thick line is the Northern Hemisphere tropopause, which is defined in this study as the +1.5 PV unit surface (or equivalently as the +1.5 PV unit contour on a θ surface), where 1 PV unit = 10^{-6} K m^2 s^{-1} kg^{-1}. The hatched region denotes a surf zone, where the meridional gradient of PV across the tropopause is regionally reversed.

the destruction of the disturbance's wavelike attributes and the transformation of its associated PV contours into a pattern such as that shown in Fig. 1.

The theory of nonlinear critical layers provides an explanation for the flow evolution within a Rossby wave critical layer (e.g., Stewartson 1978; Warn and Warn 1978; Haynes 1985; Killworth and McIntyre 1985). Insight into the flow behavior during a Rossby wave packet's approach to a critical layer, however, can be appreciated within the linear dynamical framework. In a barotropic flow with a nonuniform basic state [e.g., one composed of a latitudinally varying zonal velocity, $\overline{u}(y)$], the quasi-plane-wave solution to the linearized quasigeostrophic (QG) PV equation yields a two-dimensional Rossby wave dispersion relationship in the following form:

$$c_x - \overline{u} = -\overline{q}_y(k^2 + l^2)^{-1}, \tag{1}$$

where c_x is the wave's phase speed in the zonal direction, k and l are the zonal and meridional wavenumbers of the disturbance, and $\overline{q}_y$ is the meridional gradient of the mean QG PV. The corresponding zonal and meridional group velocity components are

$$c_{g_x} = \overline{u} + \overline{q}_y(k^2 - l^2)(k^2 + l^2)^{-2} \quad \text{and} \tag{2a}$$

$$c_{g_y} = 2kl\overline{q}_y(k^2 + l^2)^{-2}. \tag{2b}$$

For a given $\overline{q}_y$ and k, when $\overline{u} \to c_x$, $|l| \to \infty$ according to (1), and consequently c_{g_x}, $c_{g_y} \to 0$ in (2). Equations (1) and (2) suggest that Rossby waves propagating toward a critical surface ''pile up'' and exhibit a change in shape during the process whereby their phase lines tilt progressively toward the zonal dimension as their meridional length scale shrinks. The PV contour in Fig. 1, which portrays a breaking Rossby wave over the west Pacific, has implicitly experienced aspects of this type of behavior.

Ultimately, as nonlinear effects become important, the velocity field associated with RWB drives a cascade of motion to increasingly fine scales, whereby intensification of constituent gradients and the enhancement of transport and mixing processes occur simultaneously (e.g., Haynes 1985; Juckes and McIntyre 1987; Polvani and Plumb 1992; Waugh and Plumb 1994; Norton 1994). When a Rossby wave breaks along the tropopause, therefore, properties of the stratosphere and troposphere are exchanged. Stratospheric air with high ozone, relatively high volcanic aerosol, and reduced water vapor content is entrained into the upper troposphere, while moist, relatively polluted air is entrained into the stratosphere. The RWB frequency distribution in the Northern Hemisphere (NH) summer (Jun, Jul, and Aug), shown in Fig. 2 (from PH99), thus exposes a geographical asymmetry in the exchange of mass between the stratosphere and the troposphere. The shaded regions in Fig. 2 outline locales wherein RWB along the tropopause at 350 K, during summer, most frequently occurs. These so-called surf zones delineate sectors of the subtropical atmosphere that are of great meteorological significance.

Following the innovative studies of the propagation and/or breaking of Rossby waves (e.g., Karoly 1983; McIntyre and Palmer 1984; Thorncroft et al. 1993; and others), it is logical to suggest that the RWB frequency maxima shown in Fig. 2 owe their existence to the interaction between equatorward-migrating midlatitude Rossby waves and their critical layers in the weak subtropical wind fields. However, it is also possible that the relatively frequent PV-gradient reversals in these regions are instead related to the breaking of the monsoon anticyclones (to the extent that they themselves are quasi-stationary Rossby waves that straddle the mean zero-wind line) and the irreversible deformation of the subtropical tropopause associated with this process (Chen 1995). In either instance, a detailed and methodical observational assessment of how *these* surf zones are created and/or maintained awaits further attention.

In this paper, we address this issue by focusing our discussion on a case study of the sequence of events leading to the creation of reversed PV gradients across the subtropical tropopause over the North Pacific. The reversal of PV gradients in this case exemplified the type of processes tabulated in the PH99 RWB climatology. In accord with the PH99 study, we designate the NH tropopause as the +1.5 PV unit surface (or equivalently as the +1.5 PV unit contour on an isentropic surface, where 1 PV unit = 10^{-6} K m^2 s^{-1} kg^{-1}). In the example we present, reversed PV gradients across the tropopause (with a magnitude of at least 1 PV unit per 10° latitude) first appeared at 25°N and 180° on 1200 UTC 10 June 1992, the time herein defined as ''onset.'' Our elucidation of the large-scale flow evolution during the several days prior to onset suggests that the reversal of PV gradients on 10 June was triggered by the intrusion of a midlatitude Rossby wave packet into a critical layer over the subtropical North Pacific. Air-parcel trajectories are shown to highlight the confluence of Asian monsoon outflow and stratospheric air prior to and dur-

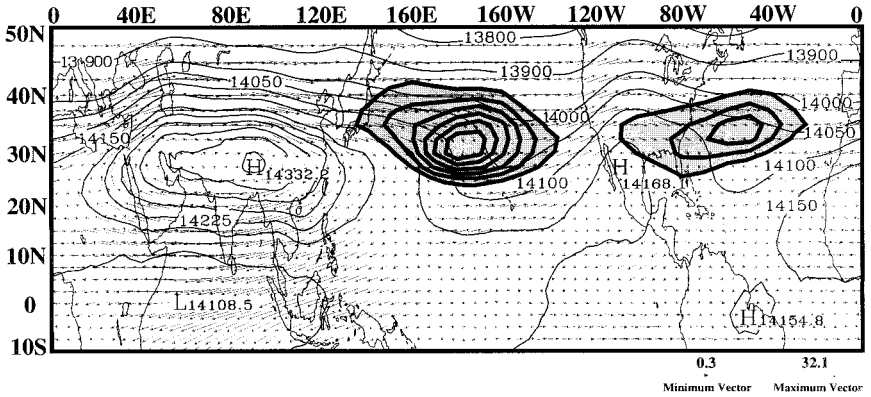

FIG. 2. Total number of reversed PV gradients across the tropopause at 350 K during the 10 boreal summers (Jun, Jul, and Aug) from 1986 through 1995. These values are contoured, by the unlabeled thick lines, from 5 by 4. The 150-hPa wind vectors (m s^{-1}) and geopotential heights (m) averaged over the same period are shown by the vectors and thin labeled contours, respectively.

ing the PV-gradient reversal, and in turn, reveal that this process united air masses with markedly different origins over the North Pacific. Composites over a set of such events during a 10-yr period are provided to augment our investigation of the processes involved in the inception of reversed PV gradients across the tropopause during the NH summer over the North Pacific. The evidence they provide upholds the notion that this surf zone is indeed related to the repeated invasion of midlatitude Rossby wave packets into the weak winds over the subtropical Pacific.

In section 2 of this paper, the data and analysis techniques are described. With explicit regard to the validity of linear theory and the Wentzel–Kramers–Brillouin–Jeffreys (WKBJ) approximation, we employ isentropic PV maps and wave activity[2] diagnostics in section 3 in our assessment of the preonset propagation characteristics of the ''precursor'' Rossby wave packet. In that section, the history of the wave activity propagation patterns associated with the packet, as well as the participation of Asian monsoon outflow in the disturbance's reversal of PV gradients over mid–Pacific Ocean, are also discussed. It should be noted that our analysis of the 10 June case indicates that much of the wave activity associated with the precursor wave packet, as it departed midlatitudes and invaded the weak wind regime in the subtropics, followed a quasi-horizontal path above 300 hPa. This is consistent with the observation (Fig. 3) that the reversed PV gradients associated with this ''RWB event'' most numerously appeared at 350 K, even though they extended across a range of isentropes from roughly 340 to 390 K. In an effort to best illustrate the precursor wave packet's approach to a critical line, we center our discussion in section 3 on the flow evolution at 350 K during the several days leading to onset. Section 3 also includes composites of the preonset flow structure to confirm that this case study exemplifies the type of processes responsible for the generation of the North Pacific surf zone shown in Fig. 2. In section 4, a summary and discussion are provided.

2. Data and analysis techniques

a. Data

This study employs meteorological data produced by the European Centre for Medium-Range Weather Forecasts (ECMWF). Generated from operational assimilation procedures, the data consist of twice-daily uninitialized globally analyzed fields of geopotential height, temperature, and horizontal wind on a 2.5° grid at all standard levels in the troposphere and stratosphere. Widespread agreement between global analyses produced by the National Centers for Environmental Prediction and the ECMWF exists over the NH extratropics (Trenberth and Olson 1988). Though this study focuses on the large-scale flow evolution in a sector of the atmosphere that is relatively poorly sampled by in situ observations (Daley 1991), our conclusions are based on scales of motion large enough to not likely be artifacts of the ECMWF model.

b. Analysis tools

The quantity

$$P = \frac{\theta_z}{\rho}\left[f - \frac{(u\cos\phi)_\phi}{a\cos\phi} + \frac{v_\lambda}{a\cos\phi}\right] \qquad (3)$$

was used to compute PV. Near the tropopause, P closely approximates Ertel's PV [cf. Andrews et al. 1987, Eq. (3.1.4)]. In (3), ρ is density, ϕ is latitude, λ is longitude, z is geopotential height, θ is potential

[2] Wave activity may be thought of as a measure of disturbance-associated air-parcel displacements, or ''waviness,'' in the PV field. It is proportional to the variance (with respect to the zonal mean) of QG PV, q, in the betaplane QG limit, where it may be approximated as $\overline{q'^2}/2\overline{q}_y$ (e.g., Edmon et al. 1980).

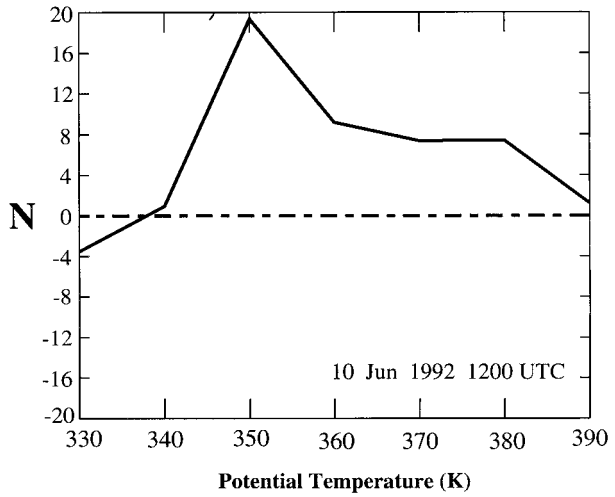

FIG. 3. The number of grid points (N) at which the magnitude of the reversed PV gradient equaled or exceeded 1 PV unit per 10° latitude on 1200 UTC 10 Jun 1992, as a function of potential temperature (θ). The search domain on each θ surface included only grid points from 140°E to 160°W and from 15° to 35°N, and included reversed PV gradients across all PV contours within that domain. Owing to the nearly continual existence of reversed PV gradients on relatively small scales in this domain during summer, N was computed as the value at onset minus the value of the 7-day mean centered at onset.

temperature, a is the earth's radius, f is the Coriolis parameter, u is the zonal velocity component, v is the meridional velocity component, and the subscripts denote partial derivatives. The derivatives in (3) were approximated by second-order-accurate centered differences. A linear interpolation was used to transform isobaric distributions of P onto isentropic surfaces. Spatial derivatives of P were also computed using second-order-accurate centered differences. Unless otherwise stated, mean values of all variables are herein defined as the 31-day time mean, centered on 8 June (2 days prior to onset), while anomalies are regarded as departures from that time mean.

The **E** fluxes (Trenberth 1986) were used to diagnose the Rossby wave propagation characteristics prior to onset. Owing to its derivation from a time-mean flow, rather than a zonal-mean flow, the **E** flux may be regarded as a three-dimensional Eliassen–Palm (EP) flux. The orientation of **E** vectors reveals the relative magnitudes of the eddy heat and momentum transports, as well as information regarding the group velocity of the Rossby waves associated with these transports. The **E**-flux divergence denotes the extent to which the eddy heat and momentum fluxes together accelerate the mean horizontal flow.

There are two three-dimensional vectors associated with the **E** flux. Since the magnitude of the time-mean zonal flow nearly everywhere in the region of interest greatly exceeded the magnitude of the time-mean meridional flow, the vector associated with the eddy forcing of the mean zonal flow, $\mathbf{E_u}$, is considered here. The global analyses' lack of precision in the vertical motion field over the relatively data-sparse subtropical oceans favors the use of the QG, spherical-coordinate version of the $\mathbf{E_u}$ vector for the present purposes. The term omitted from the primitive equation version of the $\mathbf{E_u}$ flux involves the eddy vertical velocity.

The mathematical development of the $\mathbf{E_u}$ flux yields the following expressions:

$$\frac{d\overline{u}}{dt} \propto \frac{1}{\cos\phi}\nabla \cdot \mathbf{E_u}, \tag{4}$$

where

$$\mathbf{E_u} = \left[\frac{1}{2}(\overline{v'^2} - \overline{u'^2}),\ -\overline{u'v'},\ f\frac{\overline{v'\Phi_z'}}{S}\right]\cos\phi,$$

$$\nabla = \left[\frac{\partial}{\partial x},\ \frac{1}{\cos\phi}\frac{\partial}{\partial y}\cos\phi,\ \frac{1}{\rho_0}\frac{\partial}{\partial z}\rho_0\right], \quad \text{and}$$

$$\frac{d}{dt} = \frac{\partial}{\partial t} + u\frac{\partial}{\partial x} + v\frac{\partial}{\partial y}. \tag{5}$$

In these expressions, the overbars symbolize a time mean. The eddies, denoted by the primes, are departures from the time mean. Using standard notation, $dx = a\cos\phi d\lambda$, $dy = ad\phi$, $z = \ln(p_0/p)$, p is pressure, $p_0 =$ 1000 hPa, $\rho_0(z) = \rho_s e^{-z}$, ρ_s is the density at the surface, Φ is the geopotential, $\Phi_z = RT$, R is the ideal gas constant, T is temperature, S is the static stability given by $S = R[T_z + \kappa T]$, $\kappa = R/c_p$ and c_p is the specific heat at constant pressure of dry air. In addition, a, ϕ, λ, and f are the same as in (3). A linear interpolation was used to estimate S and the vertical divergence of $\mathbf{E_u}$.

According to (4), wherever the $\mathbf{E_u}$ flux is convergent (divergent), the eddy forcing tends to decrease (increase) the mean zonal wind. This holds for all transient QG eddies, whether linear or nonlinear, wavelike or turbulent (Edmon et al. 1980). To the extent that WKBJ theory applies, and given that the mean zonal gradient of absolute vorticity is small, $\mathbf{E_u}$ also denotes a flux of wave activity whereby the pattern of arrows representing $\mathbf{E_u}$ is parallel to the intrinsic group velocity of the eddies.

In this study, RWB onset is defined as ''day[0],'' and ''day[t]'' refers to t days relative to onset. The compositing technique we employed was based on the designation of day[0] as the RWB onset time for each event we included in our analysis. The RWB events from the PH99 climatology we included in our compositing procedure were those that occurred during the 10 boreal summers (Jun; Jul; and Aug) from 1986 to 1995, and whose onset occurred between 170°E and 170°W. During these 10 summers, PV gradients more frequently reversed in this longitude band than anywhere else in the NH at 350 K (PH99).

For each variable, x, its composite, X, was evaluated at each grid point according to the formula

$$X(t) = \frac{\sum_{i=1}^{N} x(i, t)}{N}, \quad (6)$$

where i represents the event number, N is the number of events that occurred within this longitude band (33 total), and t is the time in days relative to onset. In the compositing of PV anomalies, we defined the eddy PV for each case (at each day relative to onset) as the departure from the 31-day-mean PV centered on day[−2] of that case.

3. The North Pacific RWB event of 10 June 1992

a. On the evolution of the precursor Rossby wave packet prior to onset

Isentropic PV maps at 350 K, valid for a selection of days before and after the RWB onset of 1200 UTC 10 June 1992, are shown in Figs. 4a–d. The thick dashed lines indicate approximate axes of two prominent extrema in PV that were associated with the precursor Rossby wave packet. The clockwise-evolving northeastward surge of low PV over the western Pacific Ocean unmistakably identifies the wave breaking region. The large-scale PV-gradient reversal associated with this sequence of events over the western Pacific Ocean was not strong enough to trigger the RWB detection algorithm at 350 K (see PH99 for details) until 1200 UTC on 10 June at 25°N, 180°.

The extent to which linear wave theory described the flow behavior during the few days prior to onset, at least on the spatial scales resolved by the ECMWF analyses, is clarified by examining the nature of the PV advection associated with the event. Nearly everywhere, $|\overline{u}P'_x|$ [where P denotes the approximate form of Ertel's PV expressed by (3)] was the dominant linear term. The basic-state PV contours in the region shown in Fig. 4 were nearly aligned along latitude circles (hence, $|u'\overline{P}_x|$ was comparatively small). In Fig. 5, $|\overline{u}P'_x|$ is compared to the largest nonlinear term, $|u'P'_x|$, at 350 K on day [−2]. Across much of the western Pacific Ocean between 25° and 50°N, and throughout most of the Asian sector, $|\overline{u}P'_x|$ was at least two times larger than $|u'P'_x|$. In large parts of these zones, $|\overline{u}P'_x|$ exceeded $|u'P'_x|$ by more than fivefold.

Figure 5 suggests that the nonlinear advection of PV played a relatively weak role in the large-scale evolution of PV in these regions during the few days prior to onset. At some juncture, undoubtedly, the flow's nonlinearity was strong enough to severely contort PV contours in subtropical latitudes. Indeed, upon scrutinizing subsynoptic scales of motion in the PV evolution illustrated by Figs. 4b–d, it is apparent that rapid (timescales less than 1 day) and irreversible contour deformation occurred in close proximity to the onset location, after day[−1]. Yet, as Fig. 5 attests, the downstream tilting of phase lines poleward of 25°N and the concomitant meridional length scale contraction that are readily apparent in Figs. 4a and 4b, were primarily linear effects.

The extent to which WKBJ theory suited the flow near the PV-gradient reversal is brought to attention by Fig. 6, wherein characteristic length scales of the mean and eddy flow contributions at 350 K are uncovered. To evaluate the zonal wavenumber dependence of the time-mean flow that supported the RWB event, we spectrally decomposed the spatial distribution of PV in the zonal dimension using a discrete forward Fourier transform (e.g., Stull 1988). Figure 6a shows that the basic-state PV between 25° and 45°N was concentrated in zonal wavenumbers 1 and 2. As shown in Fig. 6b, much of the anomalous PV on day[−2] at those latitudes was focused between zonal wavenumbers 5–9. Though eddy PV from all longitudes contributed to this picture, its magnitude at these wavenumbers certainly owed part of its existence to the anomalous PV associated with the precursor wave packet over the North Pacific, given that roughly 50° of longitude separated the two principal PV maxima in that sector on day[−2] at 35°N (Fig. 4a). We also note that the zonal distance between the centers of the PV anomalies associated with the wave packet (not shown) changed relatively little during the few days prior to onset, indicating a lack of change in zonal wavenumber during that time.

Estimates of the meridional scales of the basic-state and eddy components of the flow can be extracted from Figs. 6c and 6d. In these illustrations, latitudinal profiles of the mean zonal wind ($\overline{u}$) and of the mean meridional gradient of PV ($\overline{P}_y$) are compared with the latitudinal profiles of the eddy zonal wind and of the eddy PV, respectively. In Figs. 6c and 6d, $\overline{u}$ and $\overline{P}_y$ have been averaged between 100°E and 160°W. The eddy zonal wind and eddy PV are each shown at two different longitudes (145° and 175°E) at two different times (day[−2] and day[0]), respectively, in an attempt to approximate changes in the preonset meridional scale of the wave packet during its propagation[3] across the western Pacific basin. Figure 6c suggests that a reasonable meridional length scale for $\overline{u}$ at 350 K, based on the distance between the midlatitude jet axis and either of the speed minima on its flanks, is 20° latitude. The width of the prominent maximum in $\overline{P}_y$, shown by the solid curve in Fig. 6d, suggests that this midlatitude jet's support for Rossby wave propagation extended across at least 20° of latitude.

The width of the midlatitude eddy circulation on day[−2] at 145°E, as measured by either the distance between the largest maximum and largest minimum of the eddy zonal wind (see the dotted curve in Fig. 6c), or by the width of the negative-PV anomaly in midlatitudes (see the dotted curve in Fig. 6d), approximately equaled 20° latitude as well. The dashed curves in Figs.

[3] We assumed an eastward displacement of ~15° of longitude per day for the disturbance. This value is consistent with its eastward group speed near 30°N.

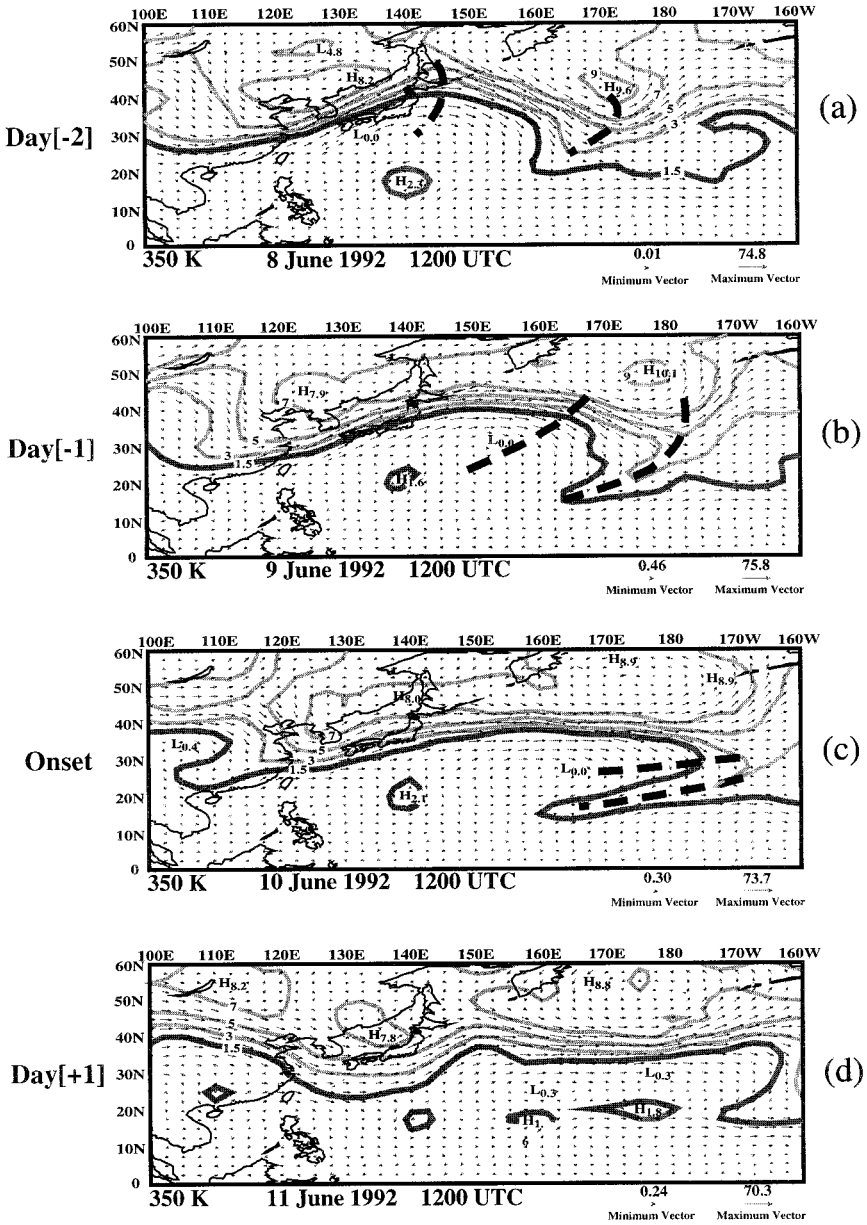

FIG. 4. Potential vorticity (PV units) and wind vectors (m s^{-1}) at 350 K for (a) day[−2] (1200 UTC 8 Jun 1992), (b) day[−1] (1200 UTC 9 Jun 1992), (c) day[0] (1200 UTC 10 Jun 1992), and (d) day[+1] (1200 UTC 11 Jun 1992). Contours are labeled. The dark contour in each plot, (+)1.5 PV units, is the tropopause. The dashed lines, provided for reference, denote approximate axes of two prominent extrema in the PV field that were associated with the precursor wave packet.

6c and 6d indicate that the meridional length scale of the eddy circulation in midlatitudes, as measured in these two ways, was closer to 10° latitude on day[0]. These illustrations suggest that the meridional width of the wave packet shrank considerably in the north–south direction after day[−2] and prior to day[0]. The evolution of PV shown in Figs. 4a–c supports this analysis. The eastward tilting of the PV extrema over the west Pacific represents a notable preonset decrease in the meridional length scale associated with the PV anomalies within the precursor wave packet.

As Figs. 6a–d attest, the length scales associated with the precursor wave packet were generally smaller than those associated with the mean flow. Both $\overline{u}$ and $\overline{P}_y$ varied over a distance as long or longer than that spanned by the individual eddies. Though WKBJ assumptions are violated in the regions and times of interest, the observations provided in Fig. 6 support the

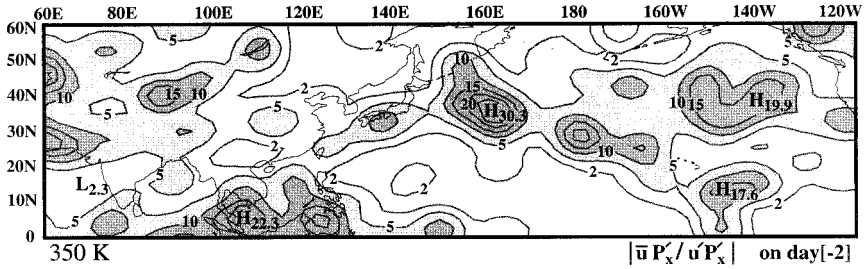

FIG. 5. The magnitude of the ratio of the linear to the nonlinear advection of the perturbation PV by the zonal wind at 350 K on day[−2]. Contours are labeled. Values between 5 and 10 are lightly shaded. Values greater than 10 are heavily shaded.

use of wave activity diagnostics to evaluate the propagation characteristics of the precursor wave activity. Indeed, WKBJ theory has been found to be at least qualitatively useful in describing Rossby wave propagation even when the properties of the mean flow change on the scale of the disturbance (e.g., Elmore and Heald 1969; Hoskins and Karoly 1981; Hoskins and Ambrizzi 1993; Sobel and Bretherton 1999).

In accord with Eqs. (2a)–(2b), the changes in shape of the precursor disturbance, as noted in the previous discussion, are indicative of a preonset accumulation of wave activity at upper levels in the subtropical latitudes over Pacific Ocean. In particular, the apparent increase in magnitude of the meridional wavenumber, $|l|$, and the steadiness of the zonal wavenumber, k, suggest that the magnitudes of both the zonal and meridional group velocities associated with the precursor wave packet (following its motion) diminished with time during the few days leading to onset.[4] The wave activity flux patterns shown in Fig. 7 confirm this expectation.

Figure 7a illustrates a Mercator projection of the horizontal components of the $\mathbf{E}_u$ vector and the three-dimensional divergence of the $\mathbf{E}_u$ flux at 350 K. For this figure, the $\mathbf{E}_u$-flux patterns, originally computed on isobaric surfaces, were linearly interpolated to the 350-K level (which resided between 250 and 200 hPa in the region of interest). In order to isolate the dynamical characteristics associated with the precursor wave packet from those associated with disturbances that tracked across the same region before and after it did, we selected a relatively short time mean about which to compute the eddy statistics. The period over which the eddy fluxes were averaged was defined as the 7 days centered on day[−2] (i.e., from day[−5] to day[+1]).

The wave activity at 350 K over the western Pacific Ocean during this time, for the most part, propagated eastward and equatorward. According to Fig. 7a, Rossby wave activity converged over the subtropical Pacific Ocean during the 7-day period surrounding 8 June. The conspicuous patches of convergent $\mathbf{E}_u$ flux that were sprinkled across the subtropical Pacific Ocean between 10° and 30°N delineate the aggregation of the southeastward propagating wave activity over the region. The shaded areas denote an $\mathbf{E}_u$-flux convergence representative of an easterly torque on the mean zonal flow in excess of 2 (m s^{-1}) day^{-1}.

Figure 7b illustrates a latitude–height cross section of the meridional and vertical components of the $\mathbf{E}_u$ vectors, as well as the three-dimensional $\mathbf{E}_u$-flux divergence pattern, averaged from 110°E to 160°W. In accordance with Fig. 7a, Fig. 7b indicates that much of the subtropical upper troposphere, in this longitudinal sector, experienced the convergence of Rossby wave activity. In this longitudinally averaged view, nearly all of the $\mathbf{E}_u$-flux convergence equatorward of 50°N that was shown in Fig. 7a was contained between 20° and 30°N and within the 400–100-hPa layer. The relative lack of eddy fluxes in the lower and middle troposphere equatorward of 40°N indicates that the wave activity associated with the precursor disturbance invaded the subtropics from midlatitudes along a quasi-horizontal path, primarily *above* 300 hPa. The heart of the wave activity transfer from midlatitudes to the subtropics, as indicated by the location of the divergence and convergence extrema, occurred between 340 and 350 K.

Much of the wave activity that converged into the subtropical west Pacific appears to have emanated from longitudes near and just east of Asia's east coast. A particularly rich wave activity source region existed near 38°N and 115°E. While this localized view in space and time nicely sequesters the propagation patterns associated with the precursor disturbance as it approached the subtropics, it reveals little about the wave activity evolution farther upstream, prior to day[−5].

In Fig. 8a, $\mathbf{E}_u$ fluxes and their three-dimensional divergence at 350 K are superposed with the anomalous PV at 350 K on 4 June. The period over which the eddy fluxes were averaged for this $\mathbf{E}_u$-flux computation was defined as the 7 days centered on day[−6], while the anomalous PV was defined as the departure from the 31-day mean centered on day[−6]. Figure 8a indicates that for at least part of the 7-day averaging period on which these $\mathbf{E}_u$ fluxes are based, eastward and southeastward wave-activity propagation patterns were col-

[4] In our definition of the basic state, $\bar{q}$, is independent of time.

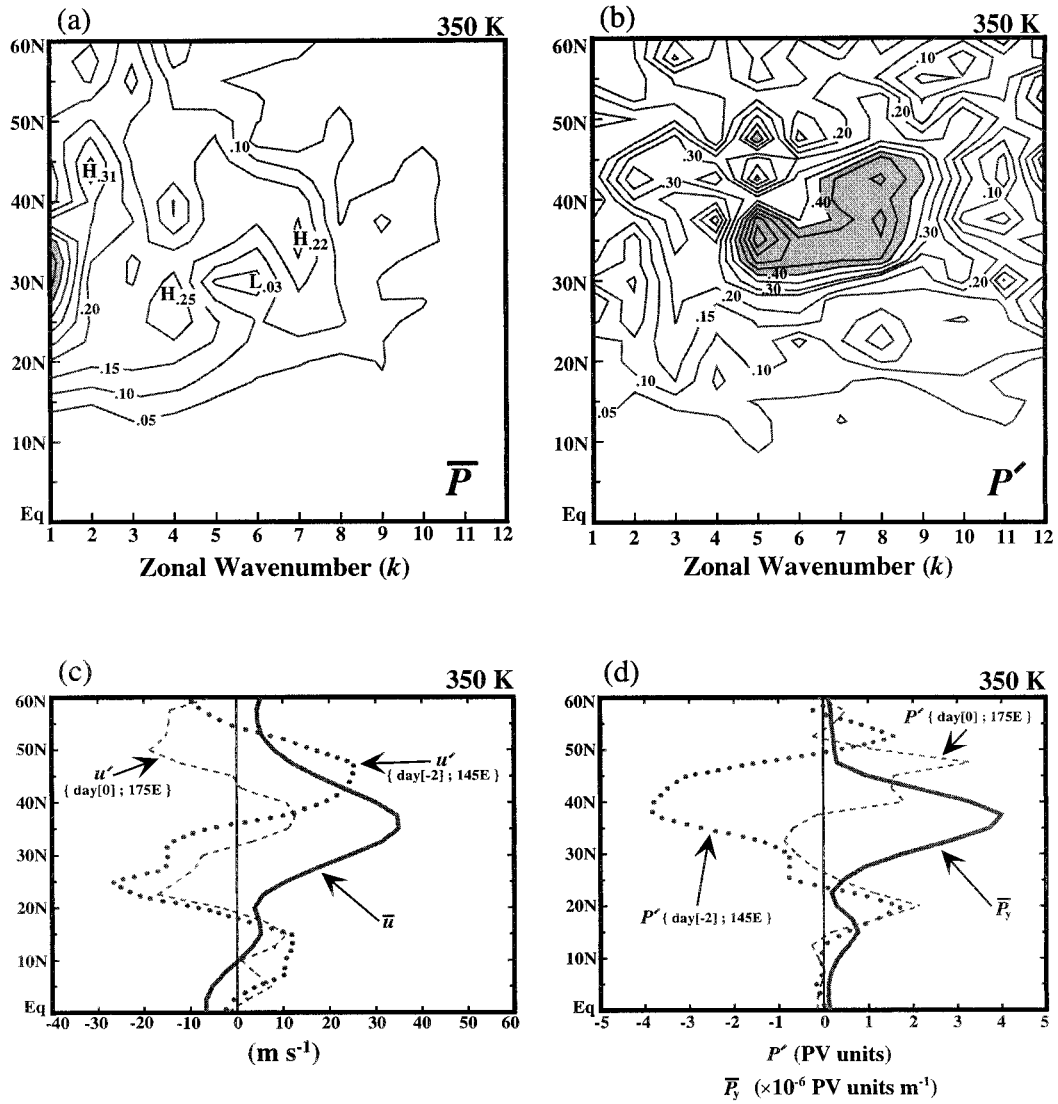

FIG. 6. (a) Zonal wavenumber dependence of the basic-state (the 31-day mean centered on day[−2]) PV as a function of latitude. (b) Zonal wavenumber dependence of the eddy (departure from the basic state) PV on day[−2] as a function of latitude. (c) Meridional profile of the basic-state zonal wind averaged between 100°E and 160°W (thick solid line), the eddy zonal wind at 145°E and day[−2] (dotted line), and the eddy zonal wind at 175°E and day[0] (dashed line). (d) Meridional profile of the meridional gradient of the basic-state PV averaged between 100°E and 160°W (thick solid line), the eddy PV at 145°E and day[−2] (dotted line), and the eddy PV at 175°E and day[0] (dashed line). Contours in (a) and (b) are labeled and in PV units. Shaded regions in (a) and (b) denote PV greater than 0.4 PV units. Zonal wind in (c) is in m s^{-1}. Units of the meridional gradient of PV in (d) are $\times 10^{-6}$ PV units m^{-1}. The eddy PV in (d) is in PV units. All variables are at 350 K.

located with a cluster of midlatitude PV anomalies over western and central Asia. These extrema in the anomalous PV field were associated with the precursor disturbance. Sequences of PV anomaly charts during this time period (not shown) confirm what Fig. 8a suggests; that the precursor wave packet propagated eastward and southeastward along the poleward edge of the Asian monsoon anticyclone (see the geopotential height field in Fig. 2 for reference), from longitudes west of 90°E.

The $\mathbf{E}_u$-vector field over central Asia also indicates that the wave activity flux at 350 K associated with the precursor disturbance propagated quasi-nondivergently across that region. The vertical structure of the $\mathbf{E}_u$ fluxes in this sector, shown in Fig. 8b, illustrates the relatively weak coupling between lower-tropospheric wave activity and the wave activity at 350 K, in the latitudinal swath occupied by the precursor PV anomalies. Much of the upward $\mathbf{E}_u$ flux from the lower troposphere, in this longitudinally averaged view, converged below 340 K and poleward of 50°N.

The transmission of $\mathbf{E}_u$ fluxes from below 700 hPa to the 350-K level, at latitudes equatorward of 50°N, occurred

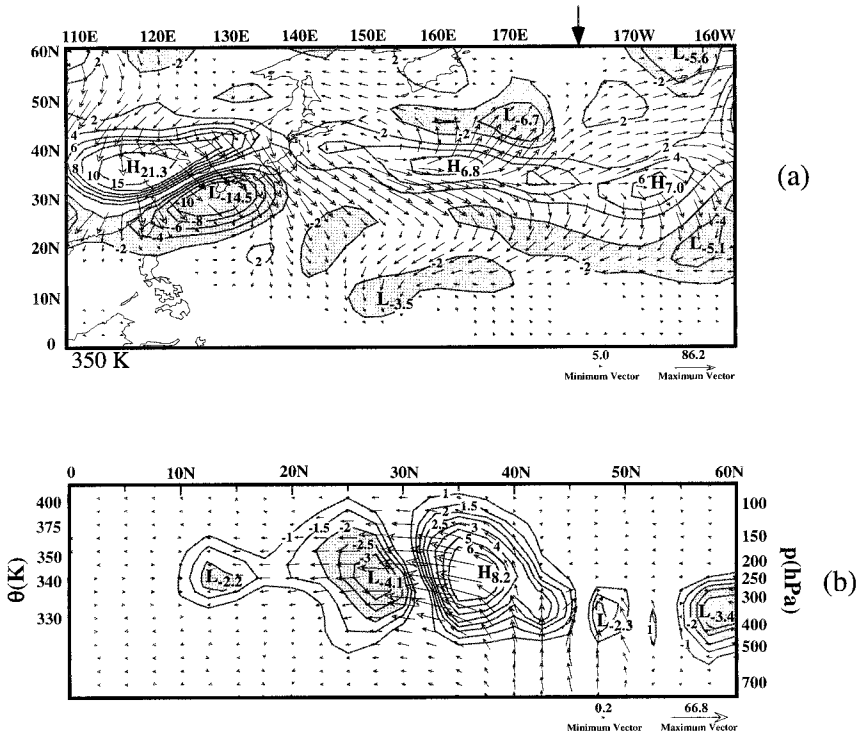

FIG. 7. (a) Three-dimensional $\mathbf{E}_u$-flux divergence [(m s^{-1}) day^{-1}] and the horizontal components of the $\mathbf{E}_u$-flux vectors (m^2 s^{-2}) at 350 K. Thick black arrow at the top of (a) points to the onset longitude. (b) Three-dimensional $\mathbf{E}_u$-flux divergence [(m s^{-1}) day^{-1}] and the meridional and vertical components of the $\mathbf{E}_u$-flux vectors (m^2 s^{-2}), in a longitudinally averaged (from 110°E to 160°W) cross section. In (b), the vertical scale on the left lists the isentropes (K) that correspond to the pressure scale (hPa) on the right, in a spatially averaged (110°E–160°W and 10°–50°N) sense on day[−2]. The $\mathbf{E}_u$-flux convergence less than −2(m s^{-1}) day^{-1} is shaded. Contours are labeled.

farther downstream during some portion of the 7 days following day[−5]. Within the longitude band and period represented in Fig. 7b, a stronger link between wave activity in the lower troposphere and wave activity near the subtropical tropopause (i.e., the precursor disturbance's establishment of a poleward heat transport) was created. This suggests that the prominent midlatitude $\mathbf{E}_u$-flux divergence maxima near the east coast of Asia and over the west Pacific at 350 K, shown in Fig. 7a (and in a zonally averaged sense in Fig. 7b), owe at least part of their existence to baroclinic growth processes. The presence of notably similar wave activity flux patterns during the latter stages of the "LC1" baroclinic wave lifecycle (Thorncroft et al. 1993) supports this claim.

b. A critical line for the precursor wave packet

Figure 9 is a Hovmöller diagram of the latitudinal-mean PV (from 25° to 50°N) at 350 K. It highlights a conspicuous zonal wavenumber and zonal phase speed (c_x) in association with the cluster of PV anomalies that defined the packet, in the 1.5–3.5-day period prior to onset. After day[−1], however, the tracks carved by these PV anomalies lost their orderly appearance. This abrupt alteration of the PV pattern was a manifestation of the extreme eastward tilting and stretching of the "middle" PV minimum (located near 145°E at day[−2]) and the concurrent advection of stratospheric PV toward its equatorward flank (see Figs. 4b,c).

For the subsequent analysis, we define c_x as the average eastward progression at day[−2.5] of the PV anomalies over the west Pacific, between approximately 110°E and the date line. The slopes of the thick black lines in Fig. 9 suggest $c_x \approx 7$ m s^{-1}. Though the following discussion assumes $c_x = 7$ m s^{-1}, use of an alternative preonset zonal phase speed that differs from c_x by 1 or 2 m s^{-1} would not notably change our conclusions.

The existence of a critical surface over the subtropical Pacific Ocean for the wave packet can be inferred from the patterns of $\mathbf{E}_u$-flux convergence noted in Fig. 7. The observed convergence of wave activity (i.e., a decrease in $|c_{g_x}|$ and $|c_{g_y}|$ following the packet's propagation), in view of the apparent preonset increase in the meridional wavenumber associated with the disturbance, suggests that the wave activity approached a region where $\overline{u} = c_x$. The similarity between the shapes of the PV contours associated with the precursor wave packet's

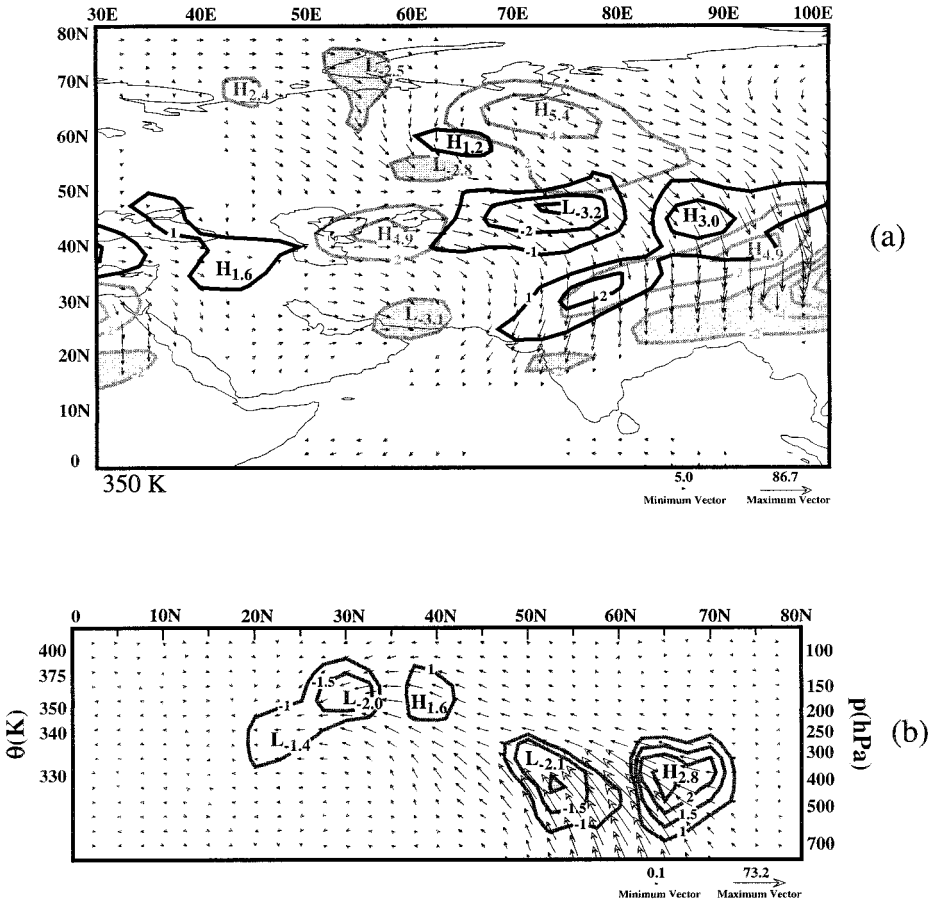

FIG. 8. (a) Three-dimensional $\mathbf{E}_u$-flux divergence [(m s^{-1}) day^{-1}], the horizontal components of the $\mathbf{E}_u$-flux vectors (m^2 s^{-2}), and anomalous PV (PV units) on day[−6], at 350 K. The $\mathbf{E}_u$-flux divergence is contoured in gray, and PV anomalies are contoured in black. (b) Three-dimensional $\mathbf{E}_u$-flux divergence [(m s^{-1}) day^{-1}] and the meridional and vertical components of the $\mathbf{E}_u$-flux vectors (m^2 s^{-2}), in a longitudinally averaged (from 30°E to 100°E) cross section. Vertical scales in (b) are identical to those in Fig. 7b, with the spatial averaging computed over the 30°–100°E and 10°–50°N domain on day[−6]. The $\mathbf{E}_u$-flux convergence less than −2(m s^{-1}) day^{-1} is shaded. Contours are labeled.

evolution, as shown in Figs. 4a–c, and PV-contour shapes obtained via analytical and numerical solutions of Rossby wave propagation into a critical layer (e.g., Stewartson 1978; Warn and Warn 1978; Juckes and McIntyre 1987) upholds this notion.

Figure 10 illustrates the distribution of $\overline{u} - c_x$ at 350 K. The zonally elongated tongue of relatively large positive values of $\overline{u} - c_x$, which extends from central Asia to the United States, represents a time-mean westerly jet wherein $\overline{u} > c_x$. Critical lines flanked this westerly jet in both midlatitudes and the subtropics. Over the subtropical Pacific, where much of the wave activity propagation associated with the precursor disturbance terminated, the $\overline{u} = c_x$ contour meandered across the 10°–22°N latitude belt. Mercator projections of $\overline{u} - c_x$ at θ -levels above and below 350 K reveal this general pattern over the Pacific Ocean. In particular, latitude–θ cross sections of $\overline{u} - c_x$ along longitudes throughout the western and central Pacific sectors (not shown) indicate that the $\overline{u} - c_x = 0$ contour exhibits a very weak isentropic dependence in the 330–390-K layer. These findings, with regard to the $\mathbf{E}_u$-flux patterns, indicate that the precursor wave packet approached a critical line over the subtropical Pacific Ocean, after departing the strong midlatitude winds over east Asia and the west Pacific.

The latitude at which the RWB detection algorithm was triggered (25°N), and the latitude (as shown in Fig. 7b) at which the longitudinally averaged $\mathbf{E}_u$-flux convergence maximized (27°N), reside north of the $\overline{u} - c_x = 0$ contour over the subtropical west Pacific. This is consistent with work by Randel and Held (1991). According to their observations, the EP flux convergence associated with equatorward migrating upper-tropospheric eddies typically lies 10°–20° of latitude poleward of their critical lines.

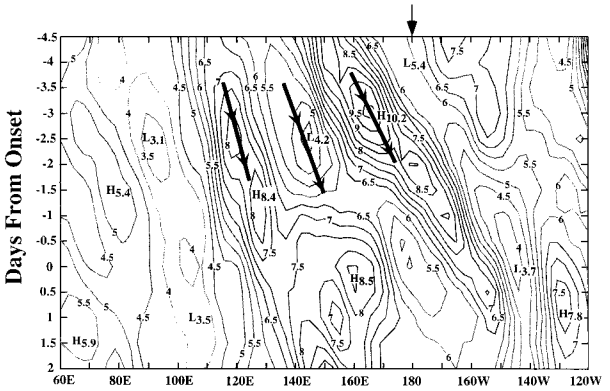

FIG. 9. Hovmöller diagram of PV (PV units) at 350 K, averaged from 25° to 50°N, for a selection of days surrounding onset. The thick solid lines with arrows delineate the progression of prominent extrema in the PV field that were associated with the precursor disturbance. These lines do not directly correspond to the dashed lines in Figs. 4a–c. Contours are labeled. The black arrow at the top of the plot points to the onset longitude.

c. Climatological flow patterns associated with the creation of the North Pacific surf zone

To suggest that the summertime surf zone over the North Pacific at 350 K, shown in Fig. 2, is related to the repeated invasion of midlatitude Rossby wave packets into the weak wind regime on the east side of the Asian monsoon, we now present illustrations of the composited PV-anomaly (PV′) patterns prior to RWB onset. Figures 11a and 11b show PV′ at 350 K on day[−1.5] and day[−0.5], composited over those boreal summer RWB events that were detected between 170°E and 170°W in the 10-yr PH99 climatology. Thirty-three RWB events were tallied during that period, within that longitude band, in the climatology. To construct these figures, anomalies were defined as departures from the 10-yr NH summer mean.

One and a half days prior to onset, as shown in Fig. 11a, a cluster of relatively strong PV′ structures appeared over Asia and the western Pacific Ocean. These midlatitude features constitute a highly averaged picture of the precursor wave packet shown in Fig. 4a. The southwest–northeast-tilted positive-PV′ structure along the east coast of Asia, the circular regions of anomalously low PV on its east and southeast flank, and the nearly meridionally oriented positive PV′ feature near 175°W are the composite versions of the PV maxima located between 120°E and the dateline in the 10 June case.

A comparison between Figs. 11a and 11b indicates that the packet of composited PV anomalies migrated eastward and equatorward with time. By day[−0.5], as shown in Fig. 11b, the maximum value of the positive-PV′ structure had moved roughly 10° east of and 5° south of its day[−1.5] position. The local minimum associated with the negative-PV′ structure to its east exhibited roughly the same eastward displacement. The absence of eddy PV in the composite, outside of the east Asian/west Pacific sector (shown clearly by Fig. 11b), suggests that the excitation of reversed PV gradients over the subtropical North Pacific is nearly exclusively associated with these eastward and equatorward migrating features.

To diagnose the average propagation characteristics associated with these disturbances, $\mathbf{E}_u$ vectors were composited over the same set of summertime RWB events. The $\mathbf{E}_u$ vectors were calculated once per event, such that the 7-day eddy-averaging period was centered at onset of each case. Figure 11c shows the composited $\mathbf{E}_u$ vectors and their three-dimensional divergence superposed on the composited mean zonal wind distribution at 350 K. In this analysis, the mean zonal winds for each case were computed as averages over the 31-day period centered at day[−2]. In a manner very similar to that shown in Fig. 7a, wave activity departed the strong midlatitude wind regime over eastern Asia and the western Pacific, and converged in the relatively weak westerly flow over the subtropical Pacific Ocean. The congruence between the highly averaged view of wave activity propagation during the few days surrounding onset, as shown in Fig. 11c, and the wave activity propagation associated with the individual case, shown in Fig. 7, further suggests that the climatological surf zone at 350 K over the North Pacific is associated with recurrent Rossby wave critical-layer interactions.

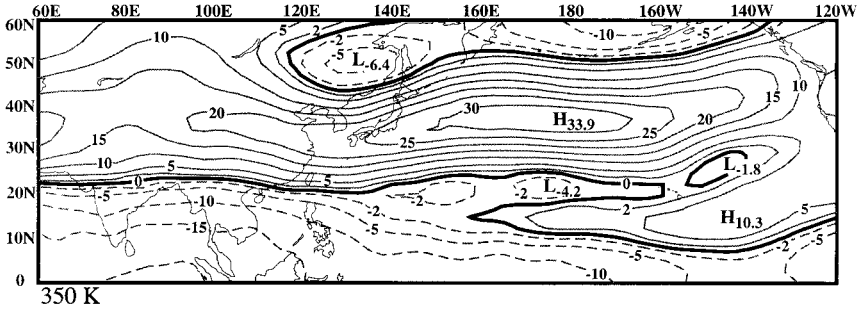

FIG. 10. Values of $\overline{u} - c_x$ (m s^{-1}) at 350 K. Contours of $\overline{u} - c_x < 0$ m s^{-1} are dashed. The thick black line is the $\overline{u} - c_x = 0$ m s^{-1} contour. For this calculation, $c_x = 7$ m s^{-1} and the mean zonal wind represents a 31-day mean centered on day[−2]. Contours are labeled.

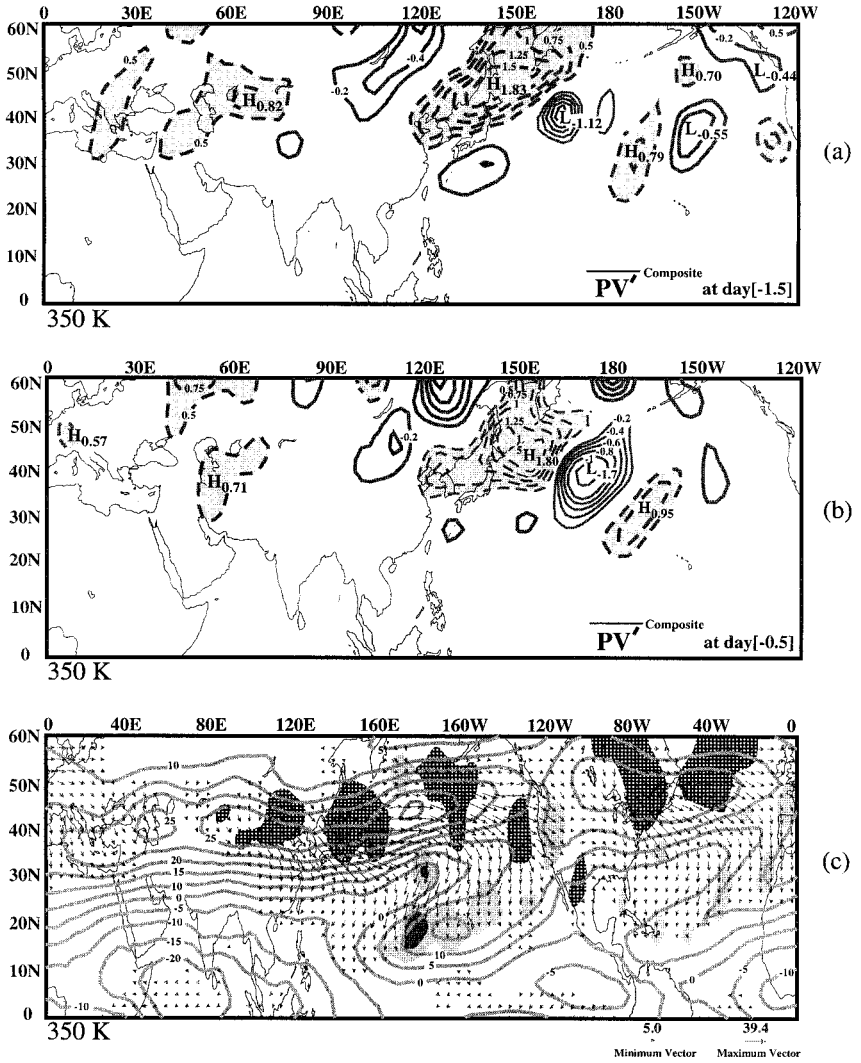

FIG. 11. (a) Composited PV anomalies (PV units) at 350 K on day[−1.5] for all boreal summer RWB events that were detected between 170°E and 170°W in the PH99 climatology. Anomalies were defined as departures from the 10-yr (1986–95) summer (Jun, Jul, and Aug) mean. Anomalous PV greater than 0.5 PV units is shaded. (b) Same as in (a) but at day[−0.5]. (c) Composited 3D $\mathbf{E}_u$-flux divergence [(m s^{-1}) day^{-1}] and the horizontal components of the $\mathbf{E}_u$-flux vectors (m^2 s^{-2}) superposed on the composited mean zonal winds (m s^{-1}) at 350 K. The $\mathbf{E}_u$-flux divergence greater than 1(m s^{-1}) day^{-1} is hatched. The $\mathbf{E}_u$-flux convergence less than −1 (−3) (m s^{-1}) day^{-1} is lightly (heavily) shaded. Contours are labeled.

The confluence of airstreams in the surf zone that is associated with many of these events is brought to attention by the following trajectory analysis for the 10 June case. A set of five isentropic trajectories at 350 K was computed for the 7-day period ending at 1200 UTC 10 June 1992 to highlight airflow paths prior to the onset of this case. The ''central'' parcel of the set was initialized at the grid point and time where the RWB detection algorithm was first activated. Four additional parcels were initialized at the same time at locations 5° latitude and 5° longitude away from the central grid point. The locations at which parcels were initialized are identified by the large dots in Fig. 12. The trajectory paths were computed from a backward integration in time (for 7 days at 1-h increments) using the horizontal wind components at 350 K. A fourth-order Runge–Kutta scheme, which employed a linear interpolation routine to retrieve the velocity field at 350 K between analysis times, was used for the integration.

The trajectory paths are illustrated in Fig. 12. The 350-K PV and winds corresponding to onset time are superposed. The trajectory scheme indicates that three of the five parcel paths, which terminated at the large dots, originated over Southeast Asia. As suggested by the Montgomery streamfunction and horizontal wind fields at the last time in the integration (not shown),

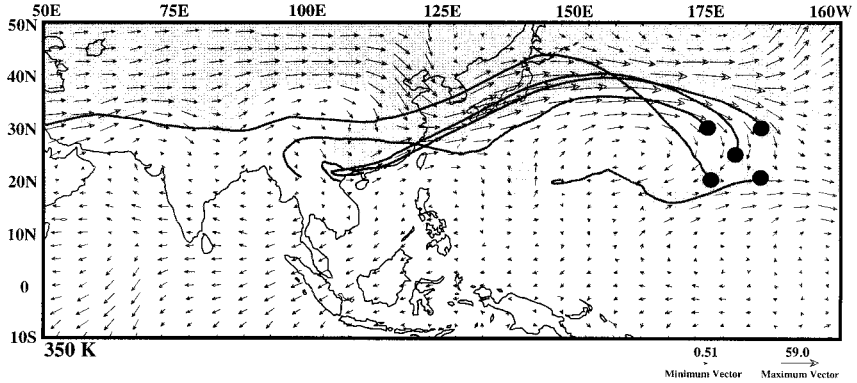

FIG. 12. Isentropic back trajectories, wind vectors (m s^{-1}), and PV at 350 K. Trajectory paths were initialized at the large solid dots at 30°N, 175°E, 30°N, 175°W, 25°N, 180°, 20°N, 175°E, and 20°N, 175°W at 1200 UTC 10 Jun 1992 and integrated backward in time for 7 days. Winds and PV are valid at 1200 UTC 10 Jun 1992. The shaded region denotes stratospheric PV (values greater than 1.5 PV units).

these three trajectories emanated from the Asian anticyclone circulation (see PH99 for details).

This process, whereby outflow from the Asian monsoon participates in the PV-gradient reversal associated with a breaking Rossby wave over the North Pacific, occurs many times each summer (PH99). In the majority (66%) of boreal summer RWB events over the North Pacific that were tabulated in the PH99 climatology, outflow from the Asian monsoon surged into the downstream surf zone. These results suggest that the northeastward expansion of upper-tropospheric air across the Asian coast, in association with a midlatitude wave packet's approach to a critical line over the subtropical North Pacific, delineates a route for the export of tropospheric air out of the Asian monsoon region into the lower stratosphere. By uniting air masses with markedly different origins, these complex flow fields associated with RWB likely modify the distribution of radiatively and chemically active trace gases that are relevant to climate change.

4. Summary and discussion

In this paper, we presented a case study of a large-scale PV-gradient reversal across the subtropical tropopause that occurred on 10 June 1992 at 25°N near the date line. Potential vorticity maps and wave activity flux patterns were employed to highlight the flow evolution leading to the onset of this RWB event (1200 UTC on 10 Jun). Roughly 1 week prior to onset, a Rossby wave packet migrated east-southeastward across central Asia at upper levels, along the jet stream on the poleward edge of the Asian monsoon anticyclone. Once the disturbance neared the east Asian coast, an upward flux of wave activity was noted, suggesting that baroclinic growth processes were likely contributors to the subsequent transport of wave activity from midlatitudes toward the subtropics across the western Pacific basin. Following its departure from eastern Asia, much of the wave activity associated with the packet traveled southeastward along a quasi-horizontal path toward the subtropical Pacific, above 300 hPa. The larger equatorward component of the packet's group velocity at these longitudes (more so than at longitudes over central Asia) was likely a by-product of the disturbance's residence on the equatorward side of a core of strong westerly winds. The existence of large, negative C_{gy} over the Pacific basin in part reflected the basic-state flow's efforts to tilt the meridional axes of the PV anomalies associated with the disturbance toward the east (and enforce $l < 0$).

The strips of divergent $\mathbf{E}_u$ flux that stretched across the midlatitude Pacific Ocean at 350 K were collocated with mean zonal wind increases of 6 m s^{-1} from 7 to 10 June (not shown). The poleward transport of westerly momentum associated with the eastward tilting, and equatorward propagating, precursor disturbance likely contributed to these midlatitude mean flow accelerations. The convergence of $\mathbf{E}_u$ flux farther south, in view of the notable reduction in the meridional length scale of the PV anomalies within the packet during the few days leading to onset, suggested that the precursor disturbance neared a critical line over the subtropical Pacific at 350 K.

To investigate the possible existence of a critical line for the precursor system, a Hovmöller diagram of PV at 350 K was used to identify the prominent zonal phase speed associated with the PV anomalies that defined the packet in the 1.5–3.5-day period prior to onset. Our analysis of the spatial distribution of the intrinsic zonal phase speed associated with these PV anomalies strongly supported the notion that the generation of reversed PV gradients over the subtropical Pacific on 10 June was a result of the wave packet's proximity to a critical line.

During the precursor wave packet's eastward and southward trek near the tropopause, around the Asian

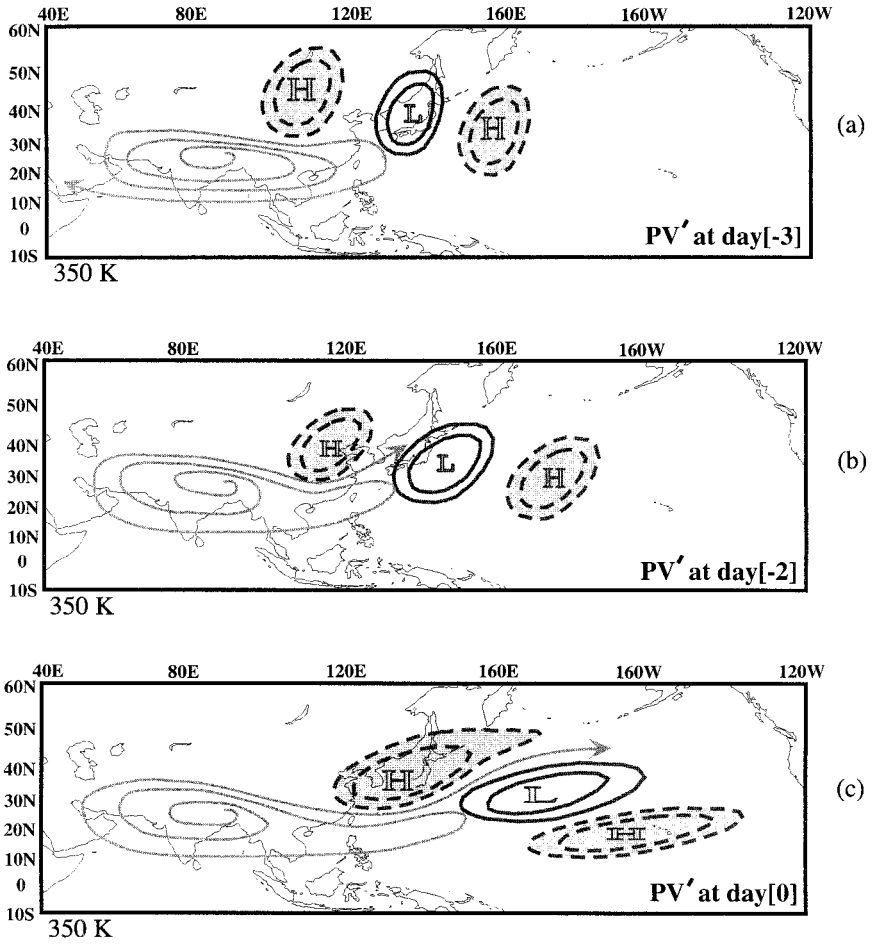

FIG. 13. Schematic depiction of the evolution of a set of PV anomalies (thick dark contours) associated with a precursor wave packet, and its interaction with the Asian monsoon (thinner gray streamline), during the several days leading to the onset of a summertime RWB event over the North Pacific. Negative PV anomalies are outlined by solid contours. Positive PV anomalies are shaded and outlined by dashed contours. The streamlines represent the upper-level anticyclonic flow associated with the Asian monsoon. Panels (a), (b), and (c) correspond to 3, 2, and 0 days prior to onset, respectively.

monsoon anticyclone's poleward and eastward periphery, outflow from the Asian monsoon was advected eastward toward the subtropical Pacific. The outflow's eventual participation in the downstream reversal of PV gradients indicates that the Rossby wave critical-layer interaction in this case united air masses of markedly different origins.

In addition to the case study, we presented composites of eddy PV and of wave activity flux patterns over a set of 33 boreal summer RWB events that occurred over the North Pacific during the 10-yr period from 1986 to 1995. These composites suggest that the surf zone in the summertime upper flow over the Pacific is intimately related to the repeated invasion of midlatitude Rossby wave packets toward their critical lines in the weak subtropical winds on the east side of the Asian monsoon anticyclone. In view of the entrainment of Asian monsoon outflow in the 10 June RWB event, we conclude that this surf zone represents a sector of the atmosphere wherein tropical tropospheric air and extratropical stratospheric air are juxtaposed during local critical-layer interactions. The climatological statistics of the reversal of PV gradients across the subtropical tropopause by Postel (1999) defend this assertion. They indicate that summertime RWB events over the North Pacific are often associated with the entrainment of strands of upper-tropospheric PV from the Asian monsoon circulation. A schematic depiction of a sequence of events associated with the creation of the North Pacific surf zone during summer is shown in Fig. 13 to compactly elucidate this process. Our analysis of the flow patterns that typically precede and accompany large-scale PV-gradient reversals across the subtropical tropopause over the North Pacific, as schematically shown in Fig. 13,

provides a straightforward conceptual model of stratosphere–troposphere exchange over this region during summer.

Finally, we noted in section 3a that, prior to the onset of the 10 June event, a coupling between the lower and upper troposphere (i.e., the establishment of a poleward heat transport) occurred in association with the precursor disturbance at some point before it departed the midlatitudes. We thereby suggested that the creation of reversed PV gradients in this case was a natural segment of the baroclinic wave life cycle (e.g., Edmon et al. 1980). The rarity, then, of the reversal of PV gradients across the tropopause on the 350-K surface during winter (PH99) may seem puzzling, given that baroclinic development is generally stronger and more frequent during winter. However, equatorward propagating Rossby waves near 350 K during winter are less likely to possess critical lines near the tropopause (which, at 350 K, primarily lies in the subtropics) than they are at, perhaps, latitudes farther equatorward (e.g., Waugh and Polvani 2000; Webster and Holton 1982). This is because the subtropical latitudes at which the tropopause on the 350-K surface generally resides, during winter, are largely occupied by the relatively strong winds associated with the subtropical jet stream (Postel 1999). It is apparent from this study that, during summer, equatorward propagating Rossby waves at 350 K possess critical lines near the tropopause since the subtropical winds, albeit in certain longitude sectors (see PH99), are relatively weak.

Acknowledgments. We wish to acknowledge very helpful comments made by anonymous reviewers on an early version of this paper. This work was supported by a NASA SAGE II grant (NAG-1-2162). GAP is pleased to acknowledge additional support from the McKinney Fellowship through the University of Wisconsin Foundation. The ECMWF data were acquired from the National Center for Atmospheric Research, which is sponsored by the National Science Foundation.

REFERENCES

Andrews, D. G., J. R. Holton, and C. B. Leovy, 1987: *Middle Atmosphere Dynamics.* Academic Press, 489 pp.

Chen, P., 1995: Isentropic cross-tropopause mass exchange in the extratropics. *J. Geophys. Res.,* **100,** 16 661–16 673.

Daley, R., 1991: *Atmospheric Data Analysis.* Cambridge University Press, 457 pp.

Duan, J., and S. Wiggins, 1997: Lagrangian transport and chaos in the near wake of a cylinder in the time-periodic regime: A numerical implementation of lobe dynamics. *Nonlinear Processes Geophys.,* **4,** 125–136.

Edmon, H. J., Jr., B. J. Hoskins, and M. E. McIntyre, 1980: Eliassen–Palm cross sections for the troposphere. *J. Atmos. Sci.,* **37,** 2600–2616.

Elmore, W. C., and M. A. Heald, 1969: *Physics of Waves.* Dover Publications, 477 pp.

Haynes, P. H., 1985: Nonlinear instability of a Rossby-wave critical layer. *J. Fluid Mech.,* **161,** 493–511.

Hoskins, B. J., and D. J. Karoly, 1981: The steady linear response of a spherical atmosphere to thermal and orographic forcing. *J. Atmos. Sci.,* **38,** 1179–1196.

——, and T. Ambrizzi, 1993: Rossby wave propagation on a realistic longitudinally varying flow. *J. Atmos. Sci.,* **50,** 1661–1671.

Juckes, M. N., and M. E. McIntyre, 1987: A high-resolution one-layer model of breaking planetary waves in the stratosphere. *Nature,* **328,** 590–596.

Karoly, D. J., 1983: Rossby wave propagation in a barotropic atmosphere. *Dyn. Atmos. Oceans,* **7,** 111–125.

Killworth, P. D., and M. E. McIntyre, 1985: Do Rossby-wave critical layers absorb, reflect, or over-reflect? *J. Fluid Mech.,* **161,** 449–492.

McIntyre, M. E., and T. N. Palmer, 1984: The 'surf zone' in the stratosphere. *J. Atmos. Terr. Phys.,* **46,** 825–849.

Norton, W. A., 1994: Breaking Rossby waves in a model stratosphere diagnosed by a vortex-following coordinate system and a technique for advecting material contours. *J. Atmos. Sci.,* **51,** 654–673.

Polvani, L. M., and R. A. Plumb, 1992: Rossby wave breaking, microbreaking, filamentation, and secondary vortex formation: The dynamics of a perturbed vortex. *J. Atmos. Sci.,* **49,** 462–476.

Postel, G. A., 1999: Rossby wave breaking along the subtropical tropopause. Ph.D. thesis, University of Wisconsin—Madison, 183 pp. [Available from Dr. Gregory A. Postel, Department of Atmospheric and Oceanic Sciences, University of Wisconsin—Madison, 1225 W. Dayton Street, Madison, WI 53706.]

——, and M. H. Hitchman, 1999: A climatology of Rossby wave breaking along the subtropical tropopause. *J. Atmos. Sci.,* **56,** 359–373.

Randel, W. J., and I. M. Held, 1991: Phase speed spectra of transient eddy fluxes and critical layer absorption. *J. Atmos. Sci.,* **48,** 688–697.

Sobel, A. H., and C. S. Bretherton, 1999: Development of synoptic-scale disturbances over the summertime tropical northwest Pacific. *J. Atmos. Sci.,* **56,** 3106–3127.

Stewartson, K., 1978: The evolution of the critical layer of a Rossby wave. *Geophys. Astrophys. Fluid Dyn.,* **9,** 185–200.

Stull, R. B., 1988: *An Introduction to Boundary Layer Meteorology.* Kluwer Academic, 666 pp.

Thorncroft, C. D., B. J. Hoskins, and M. E. McIntyre, 1993: Two paradigms of baroclinic-wave life-cycle behaviour. *Quart. J. Roy. Meteor. Soc.,* **119,** 17–55.

Trenberth, K. E., 1986: An assessment of the impact of transient eddies on the zonal flow during a blocking episode using localized Eliassen–Palm flux diagnostics. *J. Atmos. Sci.,* **43,** 2070–2087.

——, and J. G. Olson, 1988: An evaluation and intercomparison of global analyses from NMC and ECMWF. *Bull. Amer. Meteor. Soc.,* **69,** 1047–1057.

Warn, T., and H. Warn, 1978: The evolution of a nonlinear critical level. *Stud. Appl. Math.,* **59,** 37–71.

Waugh, D. W., and R. A. Plumb, 1994: Contour advection with surgery: A technique for investigating finescale structure in tracer transport. *J. Atmos. Sci.,* **51,** 530–540.

——, and L. M. Polvani, 2000: Climatology of intrusions into the tropical upper troposphere. *Geophys. Res. Lett.,* **27,** 3857–3860.

Webster, P. J., and J. R. Holton, 1982: Cross-equatorial response to middle-latitude forcing in a zonally varying basic state. *J. Atmos. Sci.,* **39,** 722–733.